Green Chemistry

Accepted Manuscript

This article can be cited before page numbers have been issued, to do this please use: N. Li, Y. Zheng, L. Wei, H. Teng and J. Zhou, *Green Chem.*, 2016, DOI: 10.1039/C6GC01327A.

This is an Accepted Manuscript, which has been through the Royal Society of Chemistry peer review process and has been accepted for publication.

Accepted Manuscripts are published online shortly after acceptance, before technical editing, formatting and proof reading. Using this free service, authors can make their results available to the community, in citable form, before we publish the edited article. We will replace this Accepted Manuscript with the edited and formatted Advance Article as soon as it is available.

You can find more information about Accepted Manuscripts in the author guidelines.

Please note that technical editing may introduce minor changes to the text and/or graphics, which may alter content. The journal's standard Terms & Conditions and the ethical guidelines, outlined in our author and reviewer resource centre, still apply. In no event shall the Royal Society of Chemistry be held responsible for any errors or omissions in this Accepted Manuscript or any consequences arising from the use of any information it contains.

ROYAL SOCIETY OF CHEMISTRY

rsc.li/green-chem

View Article Online
DOI: 10.1039/C6GC01327A

Green Chemistry

ARTICLE

Metal nanoparticles supported on WO_3 nanosheets for the highly selective cellulose hydrogenolysis to ethylene glycol†

nReceived 00th January 20xx,
Accepted 00th January 20xx

DOI: 10.1039/x0xx00000x

www.rsc.org/

Naixu Li, [a,]* Yu Zheng,[a] Lingfei Wei,[a] Hongcheng Teng [a] and Jiancheng Zhou [a,b,c,]*

Although the conversion of cellulose to polyols has been already well-developed, the production of the considerably valuable ethylene glycol (EG) is still challenging to date. The reaction has long relied on the design of suitable catalysts to obtain high selectivity and yield of EG. Herein, using well-shaped rectangular tungsten trioxide nanosheets as substrate, we investigate the catalytic performances of various metal supported catalysts using for converting cellulose to EG. Results show that Ru/WO_3 shall be more favorable for EG production, with the highest EG yield reaching 76.3% over 1% Ru/WO_3 nanosheet catalyst. Our characterizations and activity tests suggest that embedding of Ru nanoparticles onto the WO_3 nanosheets will lead to produce more W^{5+} active sites at the same reduction condition ($NaBH_4$ or H_2), which act as Lewis base sites promoting the glucose retro-aldol condensation reaction. Meanwhile, Ru/WO_3 catalyst holds a portion of the Ru in the form of amorphous $RuO_x^{\delta+}$ phases, which could further increase in the H^+ releasing into aqueous solution for cellulose hydrogenolysis . A possible catalytic mechanism of this hydrogenolysis process was accordingly proposed.

1. Introduction

The manufacture of fuels and chemicals from renewable biomass resources is in great demand for mitigation of energy crisis and environmental tension.[1-3] Cellulose, which can be derived from forests and agricultural waste and is also non-digestible by humans, has been considered as the biggest part of lignocellulosic biomass. In this regard, the conversion of cellulose into useful organic compounds has been a focus of many studies.[4-7] For example, fermentation with enzymes to produce ethanol, mineral bases/acids to get glucose, or with dilute acids in ionic liquids to yield 5-hydroxymethylfurfural (HMF).[8-11] However, these methods suffer from a series of problems, such as catalyst recycling and reusing. An alternative process to use solid acids catalysts has been a subject of intensive research. A recent study by Fukuoka and Dhepe showed the direct conversion of cellulose into sugar alcohols or hexitols (yield of sorbitol 31%) over a $Pt/\gamma\text{-}Al_2O_3$ catalyst.[12] Among the various chemical transformation processes, a current topic of high interest is the one-pot catalytic transformation of cellulose to ethylene glycol (EG), which is widely used in our daily life and chemical industries, such as a sweetener as a substitute for sugar in food, automobile antifreeze, and pharmaceutical industries.[13-15]

In 2008, Ji et al. for the first time reported an effective reaction route for the cellulose conversion to EG (yield of EG was up to 61%) over a Ni-promoted tungsten carbide catalyst within 30 minutes at 245 °C and 6 MPa hydrogen pressure.[16] Zhang et al. prepared a new three-dimensional mesoporous carbon supported tungsten carbide nanoparticles, which gave a full conversion of cellulose and a yield of EG up to 70.7%.[17] It was also shown that not only the forms of tungsten carbide, but also W, WO_3 or H_2WO_4 combined with noble metals (Pd, Pt, Rh, Ru and Ir) or nickel were effective for the production of EG.[18-22] To obtain EG, catalysts with tungstic compounds are excellent choices and tungsten species is highly active in promoting the selective cleavage of C-C bond of cellulose.[23, 24] Retro-aldol condensation, a most acceptable mechanism for the cleavage of C-C bond to obtain EG, and hydrogenation reaction are catalysed by tungsten species and nickel or noble metals, respectively.[18, 25-27] Thus, optimization of the metals / tungsten ratio has been proven to be crucial for obtaining high yield of EG. However, most of these metal contained catalysts were prepared by incipient wetness impregnation under rigorous preparation conditions, such as long impregnate time and reduction in a hydrogen flow with high temperature, which caused difficult to be scaled up. In addition, metal element can be deactivated due to sintering and poisoning.[28] On the other hand, all of these catalysts mentioned above need a carrier, such as SBA-15, SiO_2, AC and so on. Therefore, an easy and green procedure to produce catalysts under a relatively gentle reaction condition to give a high conversion of cellulose to EG is imperative.

In the present work we synthesized WO_3 nanosheets with square corners and high crystallinity by an organic-additive-

[a] School of Chemistry and Chemical Engineering, Southeast University, Nanjing 211189, Jiangsu, PR China. E-mail: naixuli@seu.edu.cn (N. Li), jczhou@seu.edu.cn (J. Zhou)
[b] Department of Chemical and Pharmaceutical Engineering, Southeast University Chengxian College, Nanjing 210088, Jiangsu, PR China
[c] Jiangsu Province Hi-Tech Key Laboratory for Bio-medical Research, Southeast University, Nanjing 211189, PR China
* Corresponding authors
† Electronic Supplementary Information (ESI) available. See DOI: 10.1039/x0xx00000x

View Article Online
DOI: 10.1039/C6GC01327A

free hydrothermal method.[29, 30] Catalytic performance of various metal loaded WO_3 catalysts were investigated in hydrolytic hydrogenation of cellulose into EG. Results show that the deposition of Ru on WO_3 via reduction of Ru salt precursor by $NaBH_4$ provide highest efficiency (100% cellulose conversion and 76.3% yield of EG). To the best of our knowledge, such an effective catalyst was first used in the field of cellulose conversion and achieved admirable results. More specifically, we focus on the effect of different Ru content (0.5-3%), H_2 pressure (1-5 MPa), reaction temperature (180-260 ^{o}C), and reaction time (1-5 h) on cellulose conversion and yield of EG to shed light on the role of each active factor. The interaction between Ru or $RuO_x^{\delta+}$ and WO_3 nanosheets rationalized by means of XRD, Raman spectroscopy, SEM, TEM, H_2-TPR, and XPS. Furthermore, the model of Ru supported on WO_3 for accelerated conversion of cellulose into EG, as well as the possible mechanism of the selective catalytic conversion of cellulose was proposed.

2. Experimental

2.1. Chemicals and Materials

Cellulose ($(C_6H_{10}O_5)_n$), Ruodium chloride hydrate ($RuCl_3$ xH_2O), Sodium tetrachloropalladate(II) (Na_2PdCl_4), disodium hexachloroplatinate (Na_2PtCl_6), Iridium trichloride hydrate ($IrCl_3$ xH_2O), Sodium hexachlororhodate (Na_2RhCl_4), tungsten trioxide (WO_3) and Activated charcoal (AC) were purchased from Aladdin Chemistry Co., Ltd in analytical grade. Sodium tungstate dehydrate ($NaWO_4$ $2H_2O$), Sodium borohydride ($NaBH_4$) and nitric acid (HNO_3) were purchased from the Shanghai Chemical Reagent Company in analytical grade, Ethylene glycol ($C_2H_6O_2$), 1,2-Propylene glycol ($C_3H_5O_2$), 1,2-Butanediol ($C_4H_{10}O_2$), 1,2-Hexanediol ($C_6H_{14}O_2$), glycerol ($C_3H_8O_3$) and 1,4-Butanediol ($C_4H_{10}O_2$) were purchased from Sinopharm Chemical Reagent Co., Ltd in GC-grade. All chemicals were used without further purification. Deionized water was used in the entire process of the experiment.

2.2. Synthesis of various Ru/WO_3 materials

WO_3 square nanosheets were successfully synthesized according to a simple organic additives-free hydrothermal method.[29, 30] Typically, 7 mL of 65% nitric acid was diluted in distilled water (30 ml) and stirred for 10 min. 2 g $NaWO_4$ $2H_2O$ was dissolved in 30 mL distilled water with ultrasonic treatment for 5 min and were slowly added into the above solution, which finally gave rise to a light yellow precipitate. After stirring for another 30 min, the suspension was hydrothermally treated 180 ^{o}C for 3 h. After cooling to the room temperature, the yellow product was centrifuged, washed 4 times with distilled water and dried in a vacuum oven overnight.

WO_3 supported Ru was prepared by homogenous deposition-precipitation (HDP) method. Typically, i.e. for the 1 wt.% Ru catalyst, where 1 wt.% represents the Ru content in weight percent (wt.%) of tungsten species, 1 g WO_3 nanosheets was grinded and dissolved in 25 mL distilled water with stirring, $RuCl_3$ aq. (0.1 mmol in 10 mL of water) was added dropwise into the above solution, and the mixture was stirred for 30 min at room temperature. Then, $NaBH_4$ aq. (0.32 mmol in 10 mL of ice water) was added into the mixture solution using an autosampler and the rated operating time was set to 10 min. The mixture was kept under stirring until it faded from dark blue to grey, which generally took about 4 h, then centrifuged, rinsed and dried at 80 ^{o}C for 12h. In a similar procedure, WO_3 supported Pd, Pt, Rh, Ir, and Ni were also prepared for comparison. Ru/AC catalyst was prepared based on the classical sequential wet impregnation method.

2.3 Catalyst characterization

In order to characterize the bulk structural and morphology of various catalysts, several characterization methods were conducted. Powder X-ray diffraction (XRD) patterns were recorded on a Bruker D8 Discover with Cu Kα radiation. Scans were carried out from 2 theta = 10° to 70° with 0.02° steps and 0.15s per step. Raman spectra were collected in Lab RAM HR800 confocal microscope Raman system (Horiba Jobin Yvon) and ambient conditions with 633 nm He-Ne laser with an integration time of 1 s and laser power of 1 mW. Scanning electron microscopy (SEM) was performed on a JSM-7800F microscope. Transimition electron microscopy (TEM) analysis was obtained in a Hitachi H-600 with a FEI Tecnai G2-F20. X-ray photoelectron spectroscopy (XPS) spectra were recorded using 2000 XPS system with a monochromatic Al-Kα source. The temperature-programmed reducibility of hydrogen (H_2-TPR) study of the samples was conducted in a ChemBet 3000 with a thermal conductivity detector (TCD).

2.4. Cellulose degradation experiments

All cellulose hydrogenation experiments were carried out in a stainless-steel micro autoclave (YZ-MR-100 ML), and the detailed procedure was as follows. Firstly, 1.0 g cellulose, 0.25 g catalysts, and 40 g deionized water were added to the autoclave simultaneously. Then the reactor was sealed and hydrogen-flushed for 3 times. Secondly, the reactor was filled with hydrogen to desired pressure, i.e., 1, 2, 3, 4, or 5 MPa. Finally, the reactor was maintained at 180, 200, 220, 240, or 260 ^{o}C for 1-3 h under a strong stirring. After reaction, the autoclave was cooled down to room temperature with dryer and the solid residues were filtered under reduced pressure. The catalyst was washed with deionized water, dried and recovered for the next run.

2.5. Product analysis

Samples were filtered through 0.22 μm-pore-size filters (Pall) prior to analysis. The products were analyzed by gas chromatography (GC). The gas chromatograph was equipped with an ON-Wax column (30 m × 0.32 mm; film thickness, 1.0 μm) and a flame ionization detector (FID). The high performance liquid chromatography was equipped with Shodex SC1011 carbohydrate chromatography column and refractive index detector (RID).

The conversion of cellulose is calculated according to eqn (1):

$$\text{Conversion}\ (\%) = \frac{B_{cellulose} - A_{cellulose}}{B_{cellulose}} \quad (1)$$

The polyols yields in this work can be calculated by eqn (2):

View Article Online
DOI: 10.1039/C6GC01327A

$$\text{Yield}(\%) = \left(\frac{k_i}{k_{C_6H_{10}O_5}}\right) \times \left(\frac{n_i M_{C_6H_{10}O_5}}{B_{cellulose} - A_{cellulose}}\right) \quad (2)$$

Where $B_{cellulose}$ is the weight of cellulose before the reaction; $A_{cellulose}$ is the weight of cellulose after the reaction; n_i is the molar amount of the product *i*; k_i is the carbon number in a molecule *i*; $MC_6H_{10}O_5$ is the relative molecular mass of $C_6H_{10}O_5$.

3. Results and discussion

3.1. Catalysis characterization

The crystalline structures of as-prepared WO_3 and Ru/WO_3 catalysts were analyzed by XRD (Fig. 1). The pure WO_3 is consistent with the Joint Committee on Powder Diffraction Standards (JCPDS) card number 43-1035, which confirms the formation of pure monoclinic WO_3 nanosheets with the lattice constants of a = 0.7297 nm, b = 0.7539 nm, c = 0.7688, and β = 90.91°.[29-31] Typical peaks at 2θ = 23.1°, 23.6°, 24.4°, 26.6°, 28.7°, 32.6°, 33.2°, 34.2° are observed, corresponding to (002), (020), (200), (120), (112), (022), (202), and (202) planes, respectively. No characteristic diffraction lines of metallic (or oxide) species can be detected in the supported samples with various Ru loading. Diffraction peaks corresponding to ruthenium (or oxide) could not be detected, possibly due to the relatively low concentration of Ru and its high dispersity. On the other hand, diffraction lines of ruthenium (or oxide) may be obscured by WO_3.

Raman spectrum is a powerful tool for understanding the detailed structure information. Accordingly, Raman spectra of several Ru supported on WO_3 catalysts and crystalline WO_3 nanosheets are provided in Fig. 2. For the WO_3 sample (Fig. 2a), two Raman peaks at 807 and 716 cm^{-1} could be assigned to W-O stretching and bending deformation modes of WO_3 crystalline nanosheets. The peaks at 271 and 328 cm^{-1} are ascribed to the bending vibration δ (W-O-W), which belongs to the properties of monoclinic phase of WO_3.[32, 33] These correspond to WO_3 as the XRD results revealed. For the spectrum of Ru/WO_3 samples (Fig. 2b-c), peaks assigned to WO_3 is not changed, indicating that the reduction of Ru species by $NaBH_4$ has not broken the structure of tungsten oxide.

The surface morphologies and particle size of WO_3 nanosheets and Ru supported on WO_3 catalysts were examined by SEM and TEM (Fig. 3). As shown in Fig. 3a, the pure WO_3 prepared by the hydrothermal method has a nanosheet structure with an average side length of 550 nm, and a thickness of ca.50 nm. A magnified SEM image of 1 wt.% Ru/WO_3 shown in Fig. 3b reveals little influence of Ru loading on the morphology of WO_3 nanosheets. Our characterization by HRTEM indicates that the WO_3 nanosheet is single-crystal based (Fig. 3c). The well-resolved fringes with an interplanar spacing of 0.386 nm can be indexed to the 002 *d*-spacing of WO_3. This feature is also confirmed by the selected area electron diffraction (SAED) analysis (Fig. 3d). Furthermore, TEM image of the 1 wt.% Ru loading WO_3 was also provided as shown in Fig. 3e. The sample comprises of small Ru nanoparticles (2-4 nm) that were wide dispersed over the WO_3 surface. The elemental composition of the catalyst determined by energy dispersive X-ray spectroscopy (EDX) analysis as shown in Fig. 3f confirmed the existence of Ru, W and O elements. We further investigated the elemental distribution of the Ru/WO_3 sample by energy dispersive X-ray spectroscopy (EDX) mapping analysis. Fig. 4 shows the STEM image of a selected Ru/WO_3 nanosheet and the corresponding elemental mapping images of W, O and Ru. Obviously, as shown in Fig. 4b-c, homogeneous distributions of W and O are observed in the nanosheet which is consistent with the SEM observation. The distribution of Ru with quite low density could also be observed (Fig. 4d).

Moreover, detailed TEM investigation with different metal content and the presence of the agglomerate structures were also studied. Generally, as shown in Fig. 5, Ru nanoparticles were uniformly distributed on WO_3 nanosheets after the reduction with $NaBH_4$. The size of Ru particle is about 2-4 nm for 0.5/1.0 % Ru/WO_3 (Fig. 5a-b) and about 2-6 nm for 3% Ru/WO_3 (Fig. 5c). HRTEM images of Ru (inset in Fig. 5d) shows an average lattice spacing of 0.216 nm that can be indexed to the metallic Ru (002) plane. It is also worth noting that 3% Ru/WO_3 contained aggregates (10-20 nm) of small nanoparticles (blue circle in Fig. 5b). These agglomerates were supposed to be consisting of discrete crystalline Ru (2-4 nm) and additional amorphous material. The oxygen content had a slight increase by chemical analysis in these areas, which is presumably due to the existence of oxidized Ru. Zhang et al. reported that $RuO_x^{\delta+}$ nanoparticles could be easily aggregated in oxidative atmosphere for the volatility of Ru species in oxidized form.[34] Lazaridis et al. proved that the reduction with $NaBH_4$ favoured the formation of amorphous oxygen enriched metal phases.[35]

To confirm postulated the existence of Ru in oxidation state and investigated the chemical elemental status of Ru/WO_3, XPS analysis was carried out and presented in Fig. 6. Fig. 6a presents the comparison of survey spectra of WO_3 and Ru loaded WO_3 samples. A close examination using high-resolution XPS spectra was then carried out on Ru 3d and W 4f (Fig. 6b-c). Fig. 6b (samples 1% Ru/WO_3) shows two peaks at 283.7 and 279.9 eV that can be assigned to Ru 3d3/2 and 3d5/2, respectively. Note the peak of C 1s at 284.2 eV was overlapped with that of Ru 3d3/2 and the appearance of C 1s should be a result adventitious carbon from the instrument.[36, 37] Fig. 6b (samples 3% Ru/WO_3) shows the presence of Ru species both in metallic and oxidation forms, as demonstrated by the identification of metallic Ru (283.7 and 279.9 eV) and Ru-O (281.3 eV) bands after the peak separation, which is in line with HRTEM results presented above.[35, 38] Fig. 6c shows the W 4f XPS scan of the different samples. The doublet at 38.6 and 36.5 eV are attributed to W^{6+} 4f5/2 and 4f7/2, while those at 37.9 and 35.8 eV correspond to W^{5+} 4f5/2 and 4f7/2, respectively.[23, 39] It is also noted that increased content of loaded Ru resulted in higher ratio of W^{5+} to W^{6+}. In principle, embedding of Ru nanoparticles onto the WO_3 crystals will lead to more W^{5+} active sites at the same reduction condition. What we should note here is that W^{5+} active sites act as Lewis base promoting the glucose retro-aldol condensation reaction.[18, 40]

View Article Online
DOI: 10.1039/C6GC01327A

More information on hydrogen consumption of the reduction temperature could be obtained by TPR to analyze the interactions between metal and metal oxide. The H_2-TPR curves of the catalysts are shown in Fig. 7. In Fig. 7a, the appearance of a peak at 633 °C may be related to the reduction of bulk WO_3 (VI) to WO_{3-x} (V, VI), while the other peak at 740 °C may be ascribed to the reduction of WO_{3-x} (V, VI) to WO_2 (IV).[41] Although the complete reduction of WO_3 requires temperatures higher than 627 °C, it is significantly different that the initial temperature decreases with the supported Ru. Fig. 7b shows two broad peaks between 380 and 800 °C, which could be a result of co-reduction of ruthenium and tungsten oxide species at lower temperature. Fig. 7c shows the TPR profile of the prepared 3% Ru/WO_3 catalysts. It was also noted that a small consumption around 120 °C might arise from the reduction of ruthenium oxide species.[42] The irregular trend in reduction behaviour suggested a possible electronic interaction between Ru species and tungsten oxide. Generally, when Ru and WO_3 species are in close relationship in the catalytic system, the spillover of the H• on the ruthenium sites seems to facilitate reduction of tungsten oxide.[22]

3.2. Evaluation of various catalysts

The direct conversion of cellulose into EG is a complex process, where the tungsten oxide plays a critical role in cellulose hydrogenolysis. Herein, nine different materials were prepared to investigate the role of each individual factor for cellulose conversion (Table 1). Under 240 °C and 4 MPa H_2, 70.2% of cellulose was converted after 2 h in the absence of catalyst and the major products are hexitols (Table 1, entry 1). After the addition of bulk WO_3, conversion rate slightly increased to 80.1% (Table 1, entry 2), but still having a low polyols yield. It means that WO_3 along in the reaction is not active enough in the acceleration of the hydrolysis of cellulose. It is generally known that the loading of Ru is beneficial to boosted hydrogenation. Thus, 1 wt.% Ru supported on WO_3 is chosen in the hydrolytic hydrogenation of cellulose. A high conversion rate up to 100% was gained (Table 1, entry 5). Notably, EG selectivity improved dramatically to 76.3%. In order to understand this process, 1 wt.% Ru supported on AC and 1% Ru/AC mechanically mixed with bulk WO_3 were also studied. As shown in Table 1, entry 3 and 4, a lower activity in terms of conversion rate and EG yield was achieved compared with 1% Ru/WO_3, although the yield of EG was increased up to 58.7%. On the most basic level, fabrication of active sites for the hydrogenation to those for retro-aldol condensation is of great importance. In our case, the ruthenium and tungsten active sites should also have a remarkable synergistic effect for this conversion process, as also elaborated by an earlier result.[22]

We also prepare a series of WO_3-based catalysts for the cellulose conversion, including noble metals (Pd, Pt, Ru, Rh and Ir) and nickel nanoparticles supported on the same WO_3 nanosheets. Among these catalysts, 1% Ru/WO_3 shows the highest EG yield. It is known that the Pd, Pt, Ru, Rh, Ir and Ni catalysts had quite different particle size and metal dispersion.[43] Obviously, the different yield of EG is not only related to the metal dispersion, but also because of the intrinsic reactivity and catalytic hydrogenation activity of various metals under hydrothermal conditions.

3.3. Effects of Ru loading

Generally, high Ru loading facilitates the process of hydrogenation. The effect of ruthenium content was thus studied in the Ru/WO_3 catalytic systems. A series of catalysts with different Ru contents were prepared and tested. As shown in Fig. 8, a volcano-type of EG yield within the range of Ru contents (0 wt.% - 3 wt.%) was observed. Specifically, the EG yield gradually increased from 5.3% to 76.3% as the content of Ru increased from 0 wt.% to 1 wt.%. Further increment in the Ru amount led to a slight decrease in the yield. Basically, when the Ru content is low, e.g., 0.5 wt.%, dissociation of few hydrogen molecules into atoms prompts the catalytic hydrogenation, leading to a small content of transitional substance hydrogenated into EG. An excess of Ru content (3 wt.%) enables the decreased EG yield. On the other hand, HRTEM analysis (Fig. 5a) reveals a uniform dispersion of 0.5 wt.% Ru over WO_3 after reduction with 2-6 nm in size, while highly loading induced agglomerations containing more $RuO_x^{\delta+}$ nanoparticles (see Fig. 5b and Fig. 6 for SEM and XPS results). When the Ru/WO_3 catalysts contained the amorphous $RuO_x^{\delta+}$ phases, lots of the protons can be released, which should be good for cellulose hydrogenolysis. Nevertheless, the predominant reaction pathway of the hydrogenation of cellulose to EG thus would be changed owing to the excessive Ru nanoparticles mask the active centers. Detailed discussion would be involved in following reaction mechanism part.

Clearly, there is a synergetic effect between Ru and WO_3 for catalytically converting cellulose to EG, and this effect can be maximized at a Ru loading of 1 wt.%.

3.4. Optimization of reaction conditions

The conversion of cellulose into EG was previously reported to be conducted in aqueous mediums.[13, 20, 21, 44] We therefore next sought to investigate the reaction conditions, i.e. pressure, reaction temperature and time, on cellulose degradation and the yield of EG by using 1% Ru/WO_3 catalysts. The influence of reaction pressure is shown in Fig. 9a. Other parameters including reaction temperature and time were set to constants (240 °C for 2 h). In this case, H_2 pressure significantly impacted EG yield. When the pressure was lower than 1 MPa, the freshly produced liquid was light yellow (Fig. S1a†) with an EG yield of merely 15.6%. Interestingly, after a few days, yellow liquid turned to dark brown. This transformation suggested a large amount of unsaturated bond in liquid which might be caused by the low H_2 content in the hydrogenation process. The notion was further confirmed via Fehling´s tests. It was worth pointing out that the same phenomenon was observed on the hydrogenolysis product of cellulose by using WO_3 (Table 1, entry 2). Considering the low conversion of cellulose without ruthenium species, we supposed that partly WO_3 nanosheets reduced to WO_{3-x} species in the reaction and further acted as a Lewis base for C-C cleavage via a retro-aldol condensation pathway. By increasing the H_2 pressure from 1 MPa to 4 MPa, the yellow

View Article Online
DOI: 10.1039/C6GC01327A

colour disappeared gradually (Fig. S1b†). Eventually, the obtained EG yield was up to 76.3%. The EG yield was almost unchanged if excessive H_2 pressure was applied.

As shown in Fig. 9b, the cellulose conversion is also sensitive to the changes in reaction temperature. Only 5.4% of cellulose was converted at 180 ^{o}C. The conversion rate was gradually increased when reaction temperature was elevated from 180 ^{o}C to 260 ^{o}C. Notably, the yield of EG also increased at higher temperature, yet reached a maximum value at 240 ^{o}C, beyond which, it decreased. It can be deduced that high temperature is necessary for promoting the initial hydrolysis of cellulose to small molecules. Moreover, continuous increase of temperature contributes to the increase of gas production, i.e. CO, CO_2 and CH_4, as well as glucose coking, which is significant to the production of EG. [21, 43] Evidently, the cellulose conversion and the yield of EG increased monotonously with the reaction time (Fig. 9c). We thus selected 2 h as the optimal reaction time. In a word, the optimized conditions were determined as: initial H_2 pressure of 4 MPa, reaction temperature of 240 ^{o}C and reaction time of 2 h.

Generally, two-dimensional nanostructures are usually favorable for various reactions, arising from their unique surface morphology and physical/chemical properties. This principle was further validated by evaluating the catalytic performance of three-dimensional WO_3 nanoparticles. Specifically, bulk WO_3 nanoparticles with irregular surface morphology and wide size distribution were obtained from Aladdin Chemistry Co., Ltd (see Fig. S2† for the SEM images). While such bulk WO_3 supported Ru catalysts showed a cellulose conversion rate of 100%, their selectivity on EG production was significantly reduced compared with the nanosheet supported one (*i.e.* 48.6% *vs* 76.3%). It is supposed that the nonuniform surface morphology as well as physical/chemical properties of the bulk WO_3 may lead to an altered behavior of Ru particles on the surface of WO_3 substrate, resulting in the declined selectivity of EG over the bulk nanoparticle supported Ru composite catalyst.

3.5. Reusability of the 1% Ru/WO_3 catalyst and its characterization after reaction

In order to investigate the reusability of the composite catalyst, the 1% Ru/WO_3 catalyst that possessed the most promising catalytic behaviour was washed and reused for five times. Although a small mass-loss of catalyst in each recycling test was discovered probably due to the complex reusing method, no significant decline in cellulose conversion and EG yield was observed after five successive cycles (Fig. S3†). We also analysed the catalyst after three cycles by XRD, Raman spectroscopy, SEM and TEM. No major changes in the XRD patterns (Fig. S4†) and Raman spectra (Fig. S5†) were found before and after the reaction. SEM and TEM images indicated the well-maintained WO_3 nanosheet structure and highly dispersed Ru nanoparticles, which were similar as the fresh catalysts (Fig. S6†). These results demonstrate that the WO_3 nanosheet supported Ru catalysts could be stable and reusable under the current reaction.

3.6. Proposed reaction mechanism

According to our previous research, various tungsten compounds (W, W_2C, WO_3 and H_2WO_4) have the ability for the conversion of cellulose to EG. WO_3 was the most prone to becoming the main component of tungsten species.[18, 20, 23] But there still exist some unclear points on how WO_3 promotes the transformation.

As shown in Fig. S7†, the yellow solid WO_3 nanosheets turned to dark grey after Ru loading. However, after the hydrothermal treatment under 240 ^{o}C and 4 MPa H_2 for 2 h in aqueous solution, the catalyst became blue. Blue compounds of tungsten were supposed as WO_{3-x} which was partly reduced from WO_3 and could also be easily oxidized in the air (Fig. S8†).[45] As aforementioned, the peak between 237 and 547 ^{o}C in the TPR of catalyst recycle could be ascribed to the formation of oxygen vacancies and W^{5+} species. This could take place most likely at the interface between the ruthenium species and WO_3 support (Fig. 10). HRTEM (Fig. 5) and XPS (Fig. 6) measurements suggested the co-existence of small crystalline ruthenium particles together with amorphous RuO_x $^{\delta+}$ species with aggregates (10-20 nm) composed of smaller nanoparticles. Dissociative adsorption happened between metallic Ru $^{(0)}$ nanoparticles and H_2, which spilled over to adjacent RuO_x $^{\delta+}$ species and bulk WO_3, releasing H^+ in aqueous solution and bringing about W^{5+} cations, respectively. The direct evidence for spillover was obtained by Khoobiar[46] and Rozanov *et al.* .[47] The presence of W^{5+} cations interacted with the C-O/C-C bond for either a hydrogenated pathway to scissions or a Lewis base leading to a retro-aldol condensation reaction (Fig. 11). We observed such behaviour previously in the hydrogenated of xylose to glycols catalysed by Ru/TiO_2.[48]

Based on the above discussion, a possible reaction scheme of cellulose hydrogenolysis was proposed, as illustrated in Fig. 12. In general, the hydrolysis of cellulose to sugars is the rate-determining step of the reaction and the production of EG from cellulose mainly involves the hydrogenation and retro-aldol condensation.[22, 23] Firstly, cellulose was hydrolysed to cello-oligosaccharides and glucose in the presence of both hot water and spilled H^+ from Ru/WO_3 catalyst. Secondly, glycolaldehyde formed from glucose via a retro-aldol condensation reaction and subsequently transformed into EG though hydrogenation. Simultaneously, some other reactions (Fig. 12b) could also proceed and compete with the retro-aldol condensation. Therefore, the main hinder for the enhanced EG relied on how to matchup the formation rate of glycolaldehyde and hydrogenation products. Development of Ru functionalized tungsten oxide nanosheets via direct reduction of its precursor on the surface by $NaBH_4$ is technically viable and thus supplies a potential solution. The close connection between ruthenium and tungsten species gives rise to a close interaction of active sites for hydrolysis and retro-aldol condensation reaction. In this case, the reactions shown in Fig. 12a turn out to be dominant for high yield of EG.

4. Conclusions

A series of WO_3 nanoparticles supported Ru catalysts were prepared for the selective hydrogenolysis of cellulose of EG in

View Article Online
DOI: 10.1039/C6GC01327A

aqueous solution. The selectivity to EG was dependent on various reaction parameters, such as metal species (Pd, Pt, Rh, Ru, Ir and Ni) and content (0.5-3%), reaction pressure (1-5 MPa), reaction temperature (180-260 ^{o}C), and reaction time (1-3 h). 1% Ru/WO_3 was found to be an optimal promoter with a complete conversion of cellulose and a top EG yield of 76.3%. Detailed characterization of Ru/WO_3 using several physicochemical methods indicates that the high yield of EG depends on a collective manufacture of the crystallinity and nature of the ruthenium particles, and the electronic interactions between tungsten oxide (WO_3 and WO_{3-x}) and Ru metallic sites. In addition, the presence of $RuO_x^{\delta+}$ is responsible for the generation of protons and metallic Ru is favourable for the reduction of WO_3 to WO_{3-x}. Finally, a possible catalytic reaction mechanism for the conversion of cellulose into EG over Ru/WO_3 catalyst was proposed. Further research will focus on the molecular comprehension of the complexation between cellulose and tungsten trioxide, as well as kinetic competition between glucose hydrogenation and retro-aldol condensation involved in the composite catalyst systems.

Acknowledgements

This work was financially supported by the Fundamental Research Funds for the Central Universities of China (No. 3207045403 and 3207045409), National Natural Science Foundation of China (No. 21576050), Jiangsu Provincial Natural Science Foundation of China (BK20150604) and A Project Funded by the Priority Academic Program Development of Jiangsu Higher Education Institutions (PAPD).

Notes and references

1 T. Choudhary and C. Phillips, *Appl. Catal. A*, 2011, **397**, 1-12.
2 J. C. Serrano-Ruiz, R. M. West and J. A. Dumesic, *Annu. Rev. Chem. and Biomol. Eng.*, 2010, **1**, 79-100.
3 R. Ma, W. Y. Hao, X. L. Ma, Y. Tian and Y. D. Li, *Angew. Chem. Int. Ed.*, 2014, **53**, 7310-7315.
4 I. Delidovich, K. Leonhard and R. Palkovits, *Energy Environ. Sci.*, 2014, **7**, 2803-2830.
5 Y. Sun and J. Cheng, *Bioresour. Technol.*, 2002, **83**, 1-11.
6 R. Cortright, R. Davda and J. A. Dumesic, *Nature*, 2002, **418**, 964-967.
7 K. Tajvidi, P. J. Hausoul and R. Palkovits, *ChemSusChem*, 2014, **7**, 1311-1317.
8 H. Fukuda, A. Kondo and S. Tamalampudi, *Biochem. Eng. J.*, 2009, **44**, 2-12.
9 J. B. Binder and R. T. Raines, *J. Am. Chem. Soc.*, 2009, **131**, 1979-1985.
10 M. Ishida, K. Otsuka, S. Takenaka and I. Yamanaka, *J. Chem. Technol. Biotechnol.*, 2005, **80**, 281-284.
11 W. S. Mok, M. J. Antal Jr and G. Varhegyi, *Ind. Eng. Chem. Res.*, 1992, **31**, 94-100.
12 A. Fukuoka and P. L. Dhepe, *Angew. Chem. Int. Ed.*, 2006, **45**, 5161-5163.
13 N. Ji, T. Zhang, M. Y. Zheng, A. Q. Wang, H. Wang, X. D. Wang, Y. Y. Shu, A. L. Stottlemyer and J. G. G. Chen, *Catal. Today*, 2009, **147**, 77-85.
14 A. Corma, S. Iborra and A. Velty, *Chem. Rev.*, 2007, **107**, 2411-2502.
15 P. De Wulf, W. Soetaert and E. J. Vandamme, *Biotechnol. Bioeng.*, 2000, **69**, 339-343.
16 N. Ji, T. Zhang, M. Y. Zheng, A. Q. Wang, H. Wang, X. D. Wang and J. G. G. Chen, *Angew. Chem. Int. Ed.*, 2008, **47**, 8510-8513.
17 Y. Zhang, A. Wang and T. Zhang, *Chem. Commun.*, 2010, **46**, 862-864.
18 K. Fabičovicová, O. Malter, M. Lucas and P. Claus, *Green Chem.*, 2014, **16**, 3580-3588.
19 Z. Tai, J. Zhang, A. Wang, M. Zheng and T. Zhang, *Chem. Commun.*, 2012, **48**, 7052-7054.
20 Y. Liu, C. Luo and H. Liu, *Angew. Chem. Int. Ed.*, 2012, **124**, 3303-3307.
21 M. Y. Zheng, A. Q. Wang, N. Ji, J. F. Pang, X. D. Wang and T. Zhang, *ChemSusChem*, 2010, **3**, 63-66.
22 K. Fabičovicová, M. Lucas and P. Claus, *Green Chem.*, 2015, **17**, 3075-3083.
23 Y. Cao, J. Wang, M. Kang and Y. Zhu, *J. Mol. Catal. A: Chem.*, 2014, **381**, 46-53.
24 Z. Tai, J. Zhang, A. Wang, M. Zheng and T. Zhang, *Chem. Commun.*, 2012, **48**, 7052-7054.
25 J. Zhang, B. Hou, A. Wang, Z. Li, H. Wang and T. Zhang, *AIChE J.*, 2015, **61**, 224-238.
26 J. Zhang, X. Yang, B. Hou, A. Wang, Z. Li, H. Wang and T. Zhang, *Chin. J. Catal.*, 2014, **35**, 1811-1817.
27 R. Ooms, M. Dusselier, J. A. Geboers, B. O. de Beeck, R. Verhaeven, E. Gobechiya, J. A. Martens, A. Redl and B. F. Sels, *Green Chem.*, 2014, **16**, 695-707.
28 B. Kusserow, S. Schimpf and P. Claus, *Adv. Synth. Catal.*, 2003, **345**, 289-299.
29 N. Li, H. Teng, L. Zhang, J. Zhou and M. Liu, *RSC Adv.*, 2015, **5**, 95394-95400.
30 G. Zhang, W. Guan, H. Shen, X. Zhang, W. Fan, C. Lu, H. Bai, L. Xiao, W. Gu and W. Shi, *Ind. Eng. Chem. Res.*, 2014, **53**, 5443-5450.
31 H. G. Choi, Y. H. Jung and D. K. Kim, *J. Am. Ceram. Soc.*, 2005, **88**, 1684-1686.
32 D. G. Barton, M. Shtein, R. D. Wilson, S. L. Soled and E. Iglesia, *J. Phys. Chem. B*, 1999, **103**, 630-640.
33 R. V. Chintalapalle, S. Utsunomiya, C. Julien and U. Becker, *ECS Trans.*, 2006, **1**, 37-42.
34 Y. Zhang, X. Wang, Y. Zhu and T. Zhang, *Appl. Catal., B*, 2013, **129**, 382-393.
35 P. A. Lazaridis, S. Karakoulia, A. Delimitis, S. M. Coman, V. I. Parvulescu and K. S. Triantafyllidis, *Catal. Today*, 2015, **257**, 281-290.
36 Q. Tian, L. Zhang, J. Liu, N. Li, Q. Ma, J. Zhou and Y. Sun, *RSC Adv.*, 2015, **5**, 734-739.
37 H. Guo, H. Li, J. Zhu, W. Ye, M. Qiao and W. Dai, *J. Mol. Catal. A: Chem.*, 2003, **200**, 213-221.
38 R. Schulz, A. Van Neste, P. Zielinski, S. Boily, F. Czerwinski, J. Szpunar and S. Kaliaguine, *Catal. Lett.*, 1995, **35**, 89-106.
39 X.-L. Yang, R. Gao, W.-L. Dai and K. Fan, *J. Phys. Chem. C*, 2008, **112**, 3819-3826.
40 V. I. Pârvulescu, S. Coman, P. Palade, D. Macovei, C. M. Teodorescu, G. Filoti, R. Molina, G. Poncelet and F. E. Wagner, *Appl. Surf. Sci.*, 1999, **141**, 164-176.
41 D. C. Vermaire and P. C. van Berge, *J. Catal.*, 1989, **116**, 309-317.
42 T. Omotoso, S. Boonyasuwat and S. P. Crossley, *Green Chem.*, 2014, **16**, 645-652.
43 G. Zhao, M. Zheng, J. Zhang, A. Wang and T. Zhang, *Ind. Eng. Chem. Res.*, 2013, **52**, 9566-9572.
44 Z. Xiao, S. Jin, M. Pang and C. Liang, *Green Chem.*, 2013, **15**, 891-895.
45 R. Prins, *Chem. Rev.*, 2012, **112**, 2714-2738.

View Article Online
DOI: 10.1039/C6GC01327A

46 S. Khoobiar, *J. Phys. Chem.*, 1964, **68**, 411-412.
47 V. V. e. Rozanov and O. V. Krylov, *Russ. Chem. Rev.*, 1997, **66**, 107-119.
48 C. Hernandez-Mejia, E. S. Gnanakumar, A. Olivos-Suarez, J. Gascon, H. F. Greer, W. Zhou, G. Rothenberg and N. R. Shiju, *Catal. Sci. Technol.*, 2016, **6**, 577-582.

View Article Online
DOI: 10.1039/C6GC01327A

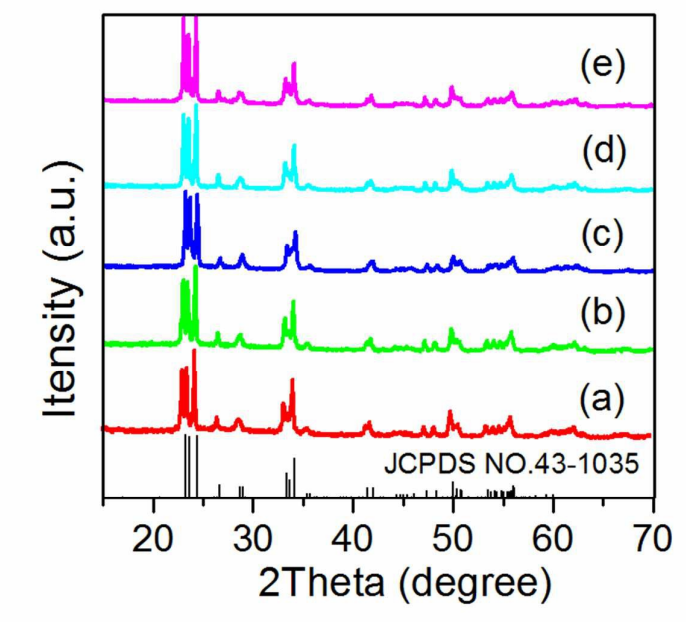

Fig. 1 XRD patterns of various catalysts: (a) WO_3, (b) 0.5% Ru/WO_3, (c) 1% Ru/WO_3, (d) 2% Ru/WO_3, (e) 3% Ru/WO_3.

View Article Online
DOI: 10.1039/C6GC01327A

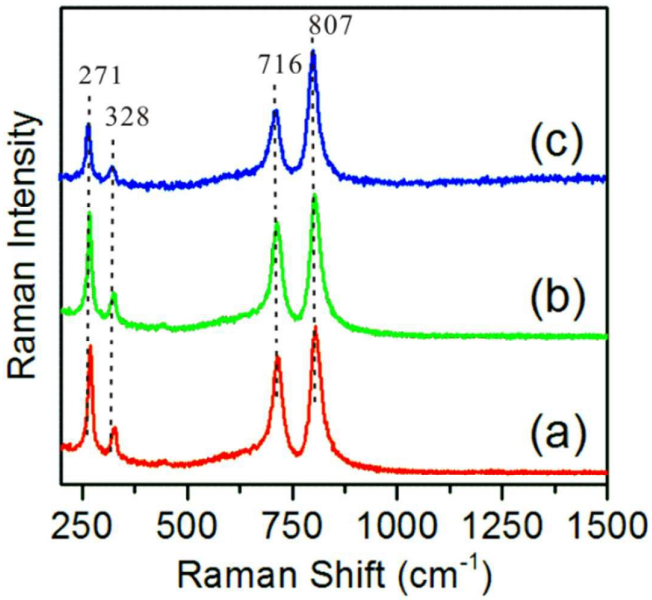

Fig. 2 Raman spectra of different catalysts: (a) WO_3, (b) 1% Ru/WO_3, (c) 3% Ru/WO_3.

View Article Online
DOI: 10.1039/C6GC01327A

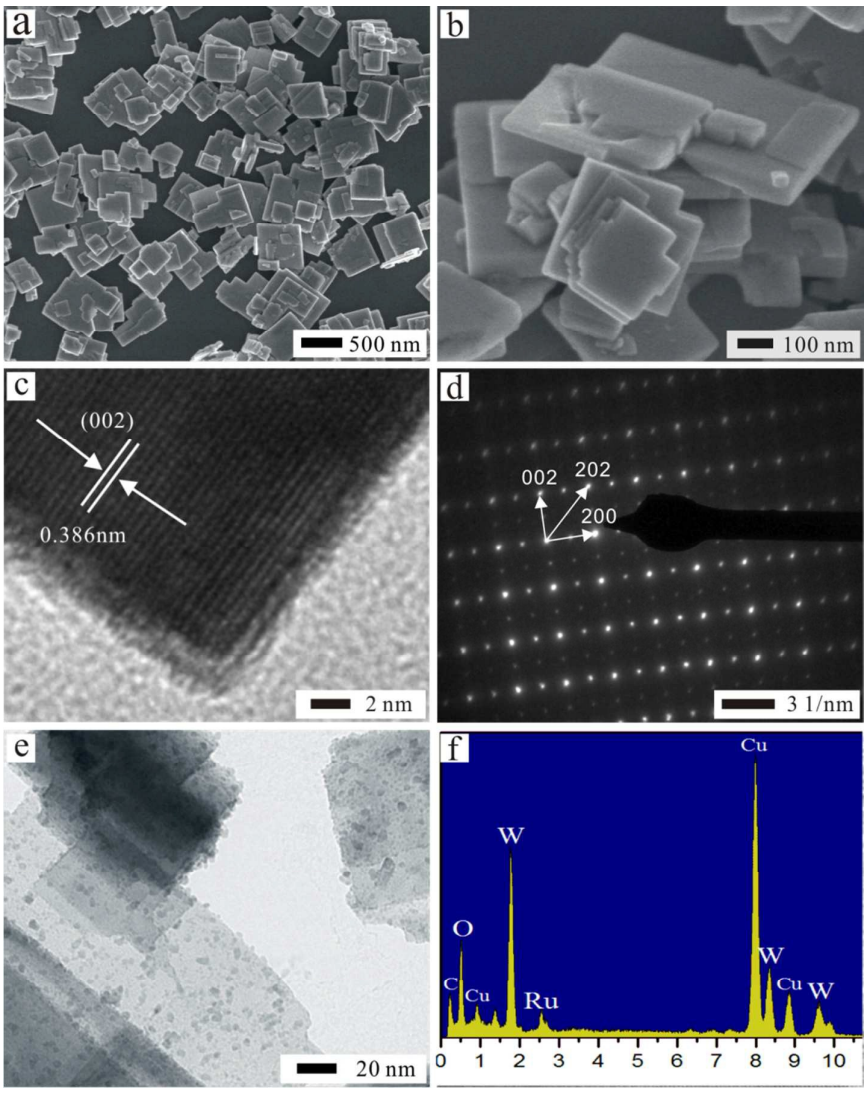

Fig. 3 (a) SEM images of WO_3, (b) SEM images of 1% Ru/WO_3, (c) and (d) are HRTEM images and corresponding SAED patterns of WO_3, (e) TEM images of 1% Ru/WO_3, (f) EDX patterns of 1% Ru/WO_3 catalyst in (b).

View Article Online
DOI: 10.1039/C6GC01327A

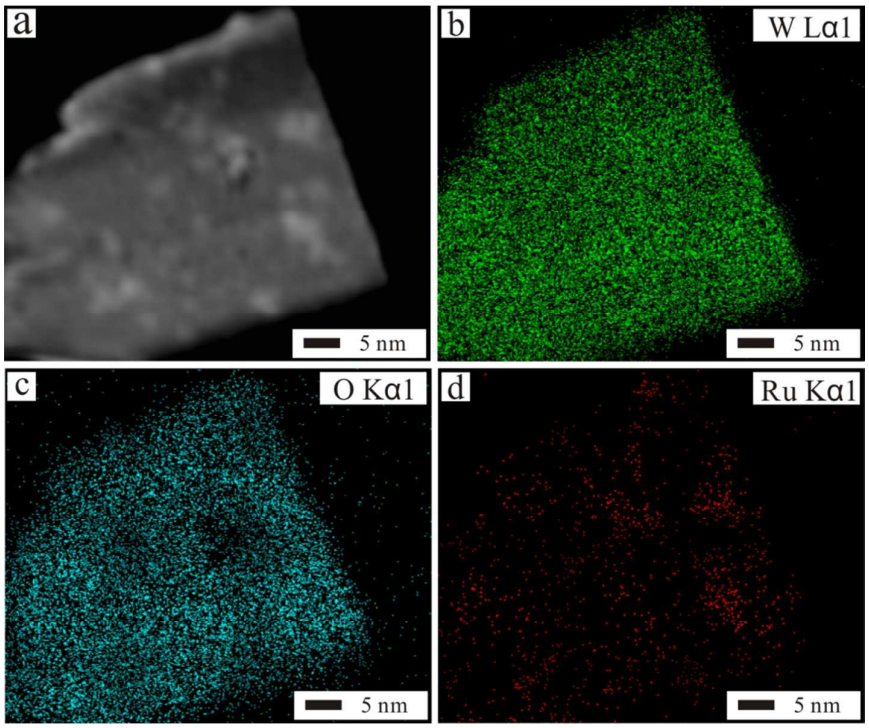

Fig. 4 (a) STEM image of 1% Ru/WO_3 and (b-d) the corresponding EDX mapping of 1% Ru/WO_3 at the region shown in (a), indicating special distribution of W, O, Ru, respectively.

View Article Online
DOI: 10.1039/C6GC01327A

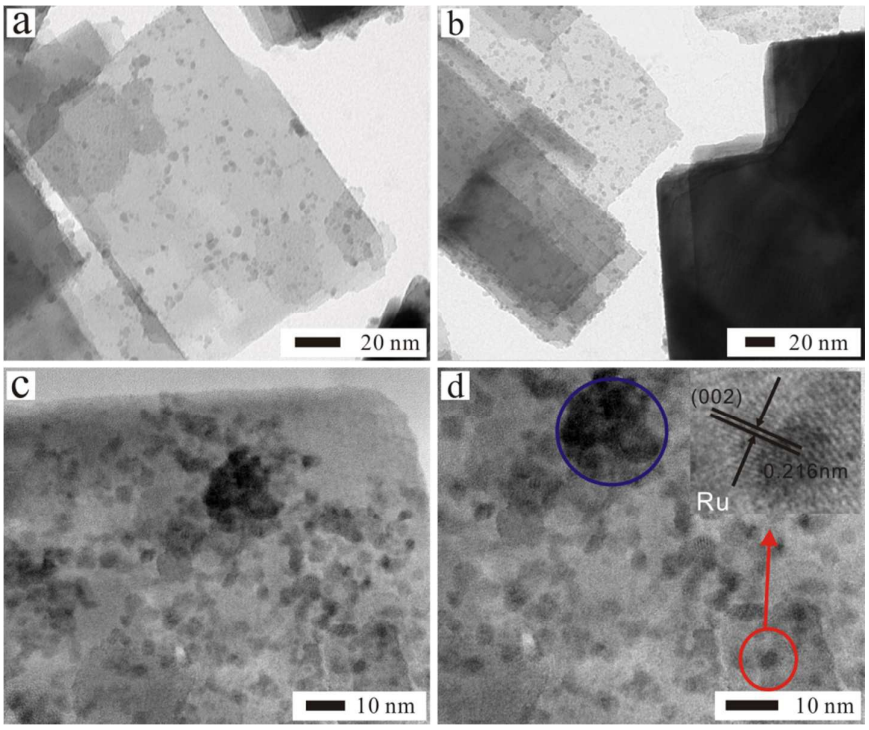

Fig. 5 TEM images of representative: (a) 0.5% Ru/WO_3, (b) 1% Ru/WO_3 and (c-d) 3% Ru/WO_3.

View Article Online
DOI: 10.1039/C6GC01327A

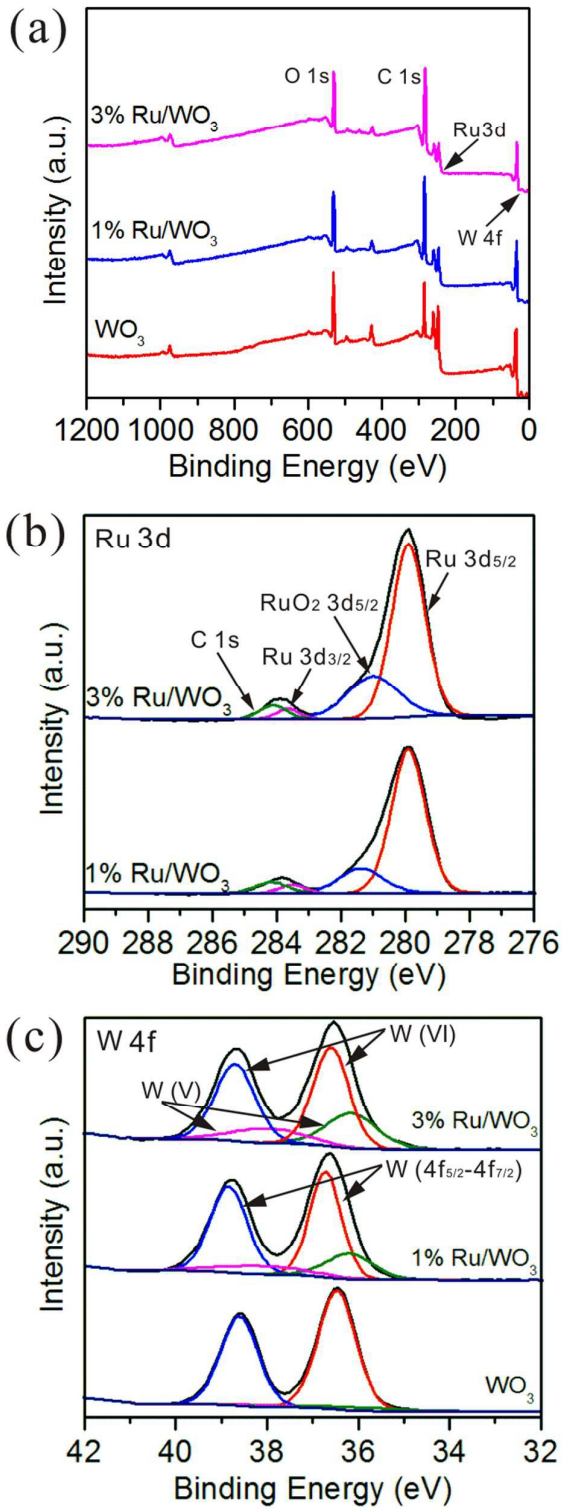

Fig. 6 (a) XPS survey spectra of sample WO_3, 1% Ru/WO_3 and 3% Ru/WO_3, (b-c) high resolution spectra of Ru 3d and W 4f.

View Article Online
DOI: 10.1039/C6GC01327A

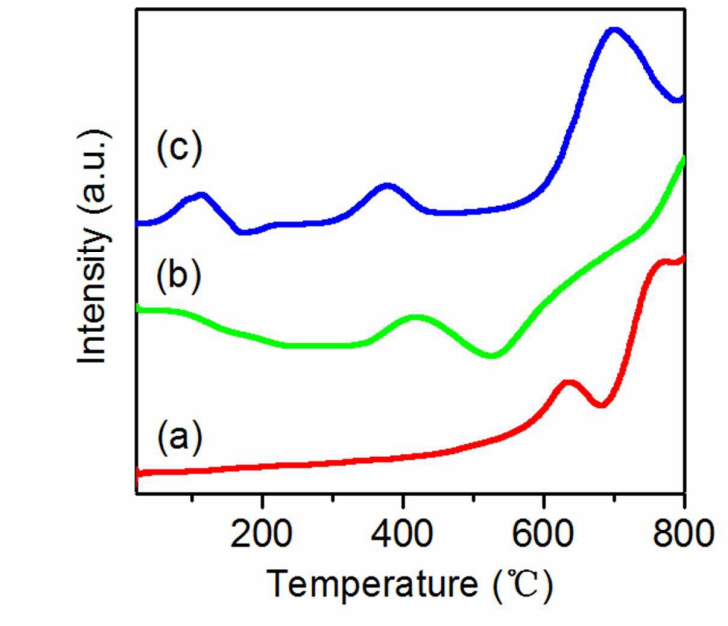

Fig. 7 H_2-TPR profiles of various catalysts: (a) WO_3, (B) 1% Ru/WO_3, (c) 3% Ru/WO_3

View Article Online
DOI: 10.1039/C6GC01327A

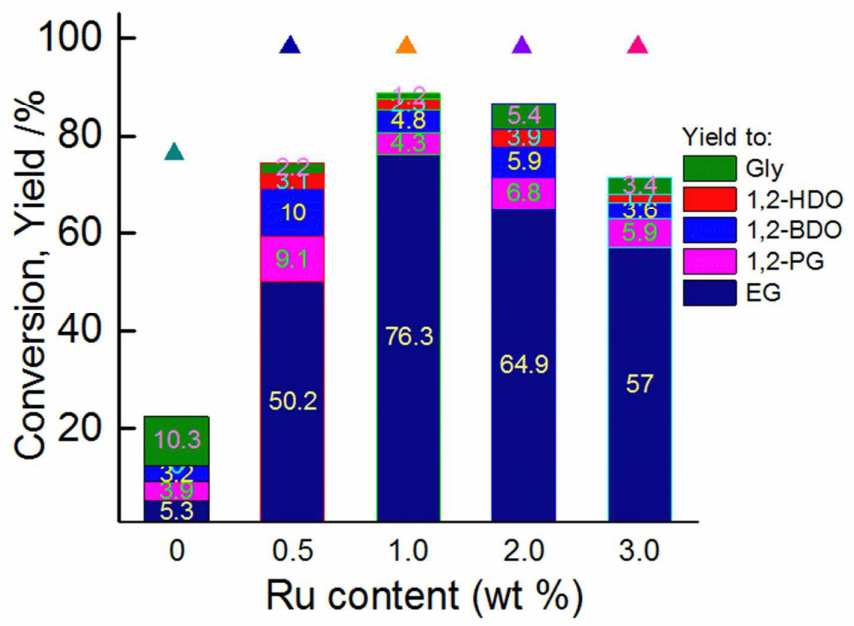

Fig. 8 The conversion of Cellulose and yield of main products with different Ru content. (reaction conditions: 0.25 g cat.; 1 g cellulose, 40 mL water, 4 MPa H_2, 240 ^oC, 2 h, 1000 rpm).

View Article Online
DOI: 10.1039/C6GC01327A

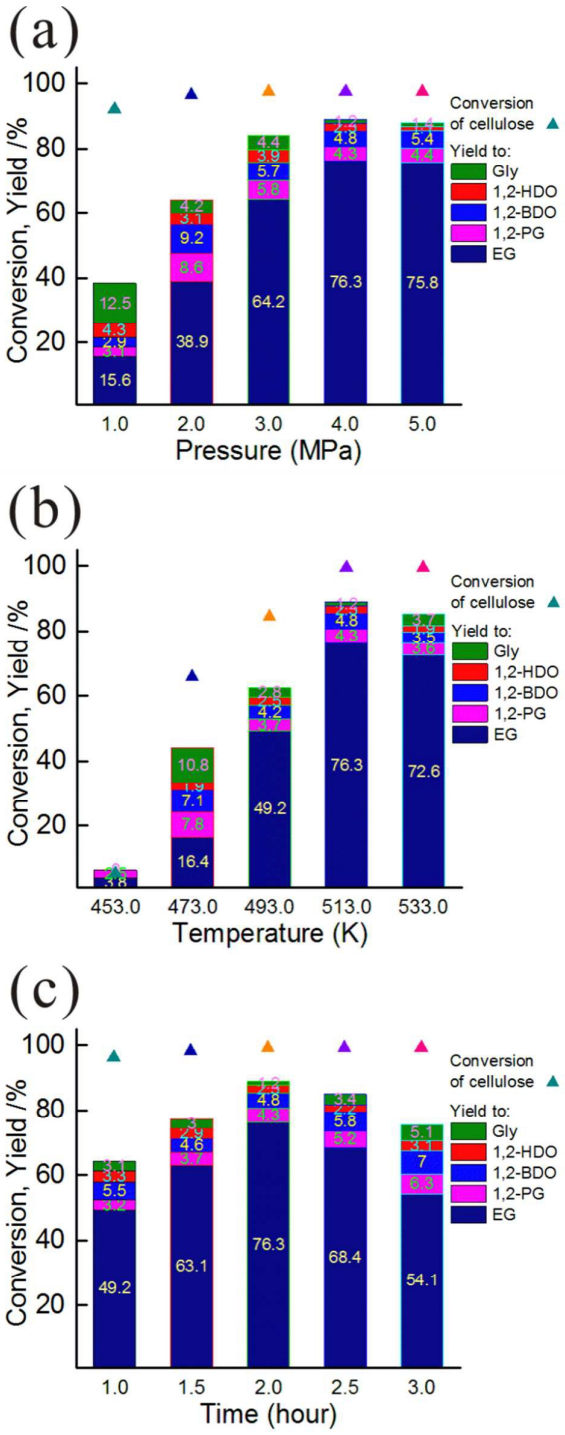

Fig. 9 Effect of reaction conditions on the conversion of cellulose and yield of main products over 1% Ru/WO_3 catalyst: (a) Effect of H_2 pressure (conditions: 240 ^oC, 2 h), (b) Effect of reaction temperature (conditions: 4 MPa, 2 h), (c) Effect of reaction time (conditions: 240 ^oC, 4

View Article Online
DOI: 10.1039/C6GC01327A

MPa).

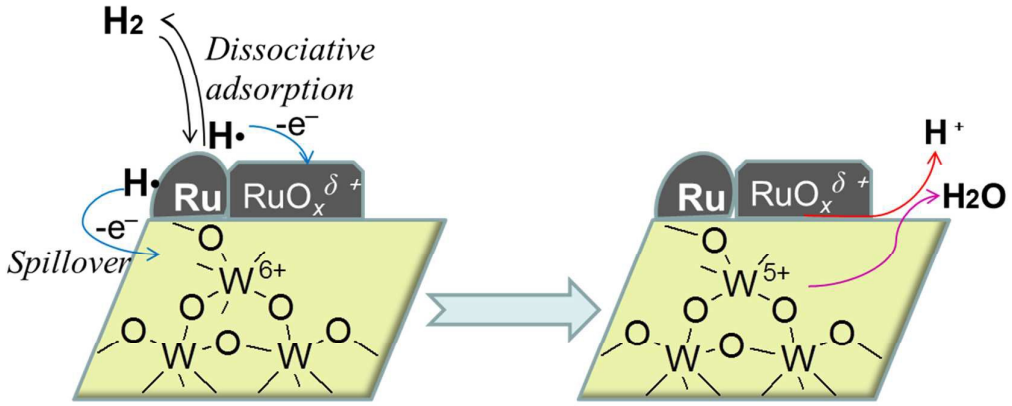

Fig. 10 Proposed model of H^+ released in aqueous solution and W^{6+} partly reduced to W^{5+} species.

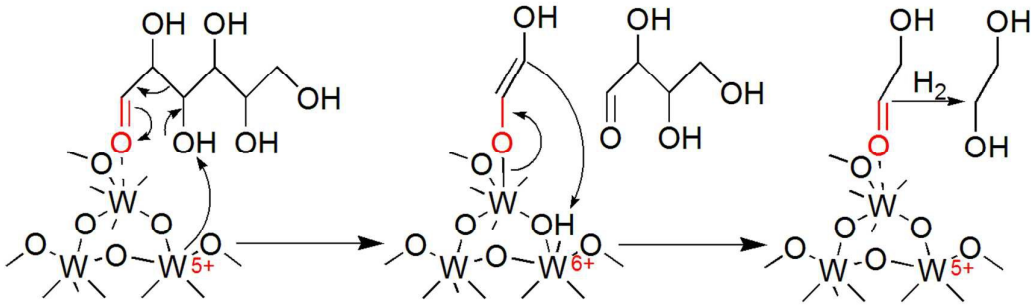

Fig. 11 W^{5+} species acting as a Lewis base for glucose retro-aldol condensation reaction to ethanol glycol.

View Article Online
DOI: 10.1039/C6GC01327A

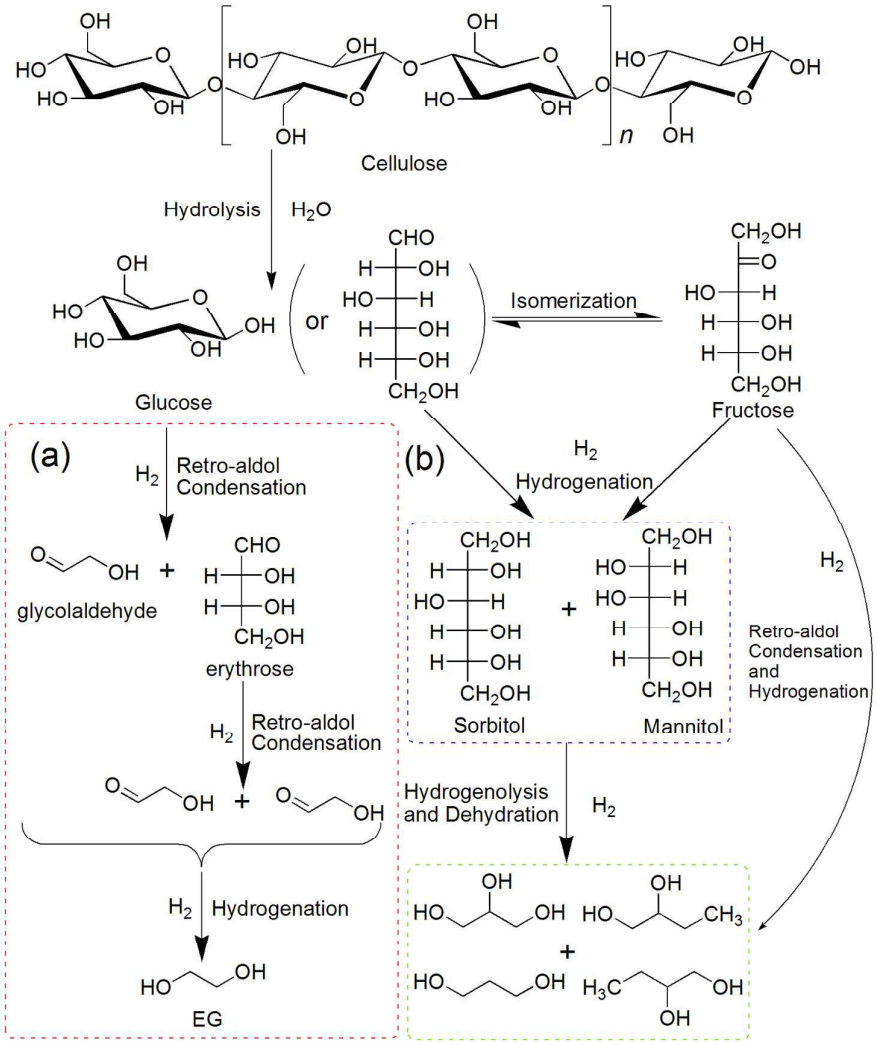

Fig. 12 Proposed reaction pathways involved in hydrolytic hydrogenation of cellulose over Ru/WO_3.

View Article Online
DOI: 10.1039/C6GC01327A

Table 1 Catalytic results of cellulose hydrogenolysis and yields of main products. [a]

#	Catalyst [b]	Conversion (%) [c]	Yield based on carbon (%) [d]				
			EG	1,2-PG	1,2-BDO	1,2-HDO	Gly
1	—	70.2	Trace	Trace	Trace	Trace	Trace
2	WO_3	80.1	5.3	3.9	3.2	Trace	10.3
3	Ru/AC	88.7	5.4	13.5	10.5	28.5	8.0
4	Ru/AC+WO_3	91.1	58.7	8.3	4.3	Trace	5.3
5	Ru/WO_3	100	76.3	4.3	4.8	2.3	1.2
6	Pd/WO_3	100	29.0	4.5	3.3	1.0	5.4
7	Pt/WO_3	99	30.1	8.4	7.2	2.4	9.0
8	Rh/WO_3	100	27.8	4.5	3.7	2.0	Trace
9	Ir/WO_3	100	25.7	5.4	4.7	3.2	5.6
10	Ni/WO_3	87.5	2.4	Trace	Trace	Trace	Trace

[a] Typical reaction conditions: 1.0 g cellulose, a designated amount of catalyst, and 40 g water were put in an 100 ml autoclave and stirred at 240 ^{o}C. [b] Metal loading (1 wt.%) is referred to nominal values of noble metals loading on the support. [c] The conversion (wt%) was calculated by the weight of cellulose before and after reaction with an uncertainty of ±3%. [d] EG, 1,2-PG, 1,2-BDO, 1,2-HDO and Gly are abbreviations of ethylene glycol, 1,2-propylene glycol, 1,2-butanediol, 1,2-hexanadiol, glycerol, respectively.

View Article Online
DOI: 10.1039/C6GC01327A

Graphic and Textual Abstract

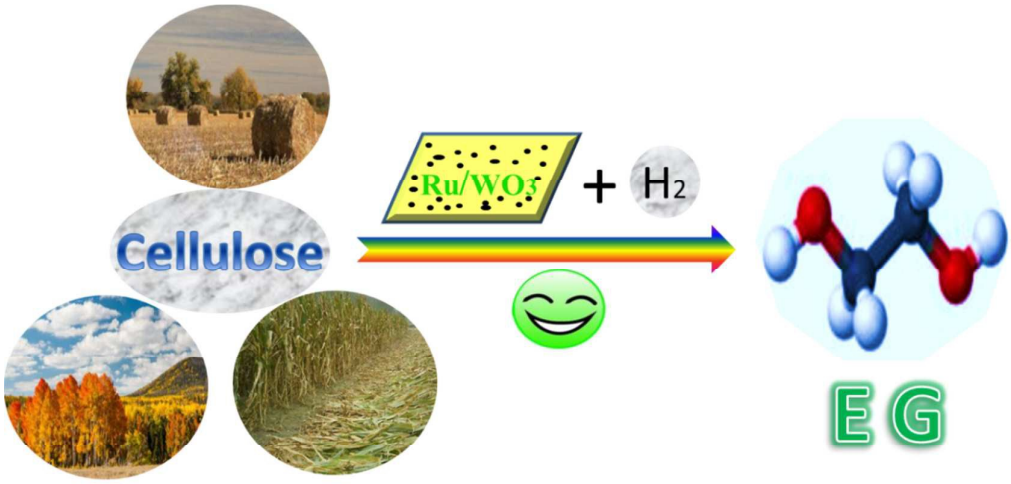

Facile synthesis of Ru supported on WO_3 nanosheets for the highly selective cellulose hydrogenolysis to ethylene glycol.